

Supporting information for

Stereochemistry of Electrophilic Attack at 34e Dimetallic Complexes: The Case of Diiron Dithiolato Carbonyls + SMe⁺

Matthew T. Olsen, Danielle L. Gray, and Thomas B. Rauchfuss*

Department of Chemistry
University of Illinois
Urbana, IL 61801
USA

Luca De Gioia and Giuseppe Zampella*

Department of Biotechnology and Biosciences
University of Milano-Bicocca
Piazza della Scienza 1
20126-Milan
Italy

Part I. Experimental Results

Improved Synthesis of [Me₃S₂]BF₄. Previous workers¹⁶ have commented on problems with the purity of [Me₃S₂]BF₄, the main impurity being [Me₃S]BF₄. We found that the purity of the product was improved if the synthesis was conducted at -45 °C rather than 0 °C. This method eliminated the minor contaminant [Me₃S]BF₄ as well as other unknown species.

To a solution of 3.310 g [Me₃O]BF₄ (Aldrich) in 15 mL of MeCN, cooled to -45 °C, was added dropwise 2.0 mL of Me₂S₂. The reaction mixture was stirred for 1 h, and then allowed to warm to 0 °C whereupon stirring was continued for 1 h. A white powder precipitated upon the addition of 25 mL of Et₂O. Yield: 3.610 g (82%).

[Me₃S₂]BAr^F₄. A mixture of 0.790 g (3.5 mmol) of [Me₃S₂]BF₄ and 2.340 (2.6 mmol) g of KBar^F₄ was pre-cooled to -45 °C and then treated with 20 mL of CH₂Cl₂. The reaction mixture was stirred for 30 min. The slurry was filtered and the insoluble residue was washed with 20 mL of additional CH₂Cl₂ which was added dropwise to minimize warming. The filtrate was removed from the cold bath and immediately

concentrated *in vacuo* to about 15 mL; in this way the removal of solvent kept the reaction mixture cold. The thick translucent mixture was then cooled again to -45 °C and a white powder was precipitated upon the addition of 30 mL of hexane. Yield: 2.460 g (98% based on KBAr^F₄). ¹H NMR (CD₂Cl₂): δ 7.72 (m, 8H, BAr^F₄⁻), 7.57 (bs, 4H, BAr^F₄⁻), 3.21 (s, 6H, [(Me₂S)SMe]⁺), 2.89 (s, 3H, [(Me₂S)SMe]⁺). Anal. Calcd for C₅₃H₂₁BF₂₄S₂ (found): C, 43.23 (41.8); H, 2.18 (2.3); N, 0 (0.0).

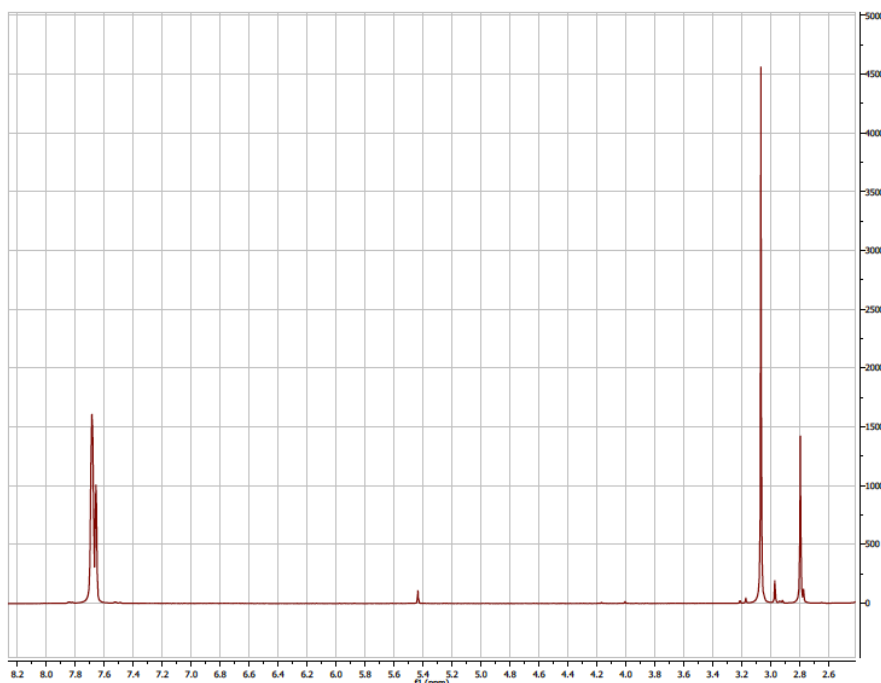


Figure SI-A1. 500 MHz ¹H NMR spectrum (CD₂Cl₂, 20 °C) of [Me₃S₂]BAr^F₄.

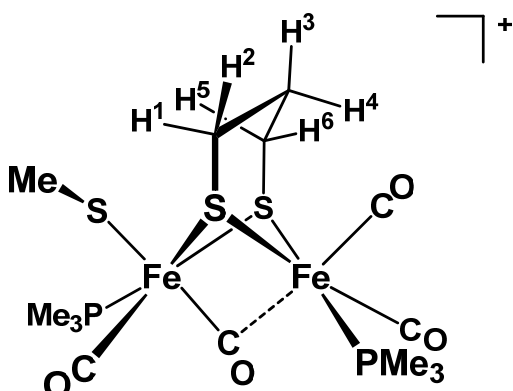
[Fe₂(pdt)(t-SMe)(CO)₄(PMe₃)₂]BAr^F₄. A solution of 0.250 g (0.52 mmol) of Fe₂(pdt)(CO)₄(PMe₃)₂ in 10 mL of CH₂Cl₂ was cooled to -78 °C. To this mixture was dropwise added a solution of 0.500 g (0.51 mmol) of [Me₃S₂]BAr^F₄ in 20 mL of CH₂Cl₂. After the addition, the mixture was stirred for 3 h. IR spectra of aliquots of the dark green reaction mixture at this stage indicated the presence of the product. The greenish solution was concentrated without external cooling to ~10 mL *in vacuo*; the temperature of the solution being kept cold by the evaporation process. A green powder precipitated upon the dropwise addition of 30 mL of uncooled hexane. The product was collected by filtration from the pale orange supernatant (assumed to contain traces of unreacted Fe₂(pdt)(CO)₄(PMe₃)₂). This crude solid was cooled to -78 °C and treated dropwise with

about 15 mL of CH₂Cl₂ followed by the addition of about 4x the volume of hexane, also added dropwise. This reprecipitation was repeated until the supernatant was clear to pale green in color - about 2-3 reprecipitations were needed. The crude yield at this stage was 0.651 g (90%). While immersed in a -78 °C cold bath, the crude product was extracted into 30 mL of Et₂O, which was added dropwise (from a room-temperature reservoir), and this extract was quickly filtered through a 4-cm plug of Celite (room temperature), rinsing with 30 mL of Et₂O. A green powder precipitated upon the addition of 70 mL of pentane. Yield: 0.469 g (72%).

Single crystals suitable for X-ray diffraction were grown by the diffusion of hexanes into CH₂Cl₂ solutions while stored at -30 °C in the dark. After ~4 weeks, dark green blocks had formed. ³¹P{¹H} NMR (CD₂Cl₂): δ 21.8 (d, *J*_{P-P} = 9, PMe₃), 16.9 (d, *J*_{P-P} = 9, PMe₃). IR (CH₂Cl₂, cm⁻¹): ν_{CO} = 2051, 2031, 2006, 1895. ¹H NMR (CD₂Cl₂): δ 7.71 (m, 8H, BAr^F₄), 7.56 (bs, 4H, BAr^F₄), 2.97 (m, 1H, S₂C₃H₆-H²), 2.74 (dq, *J* = 15, 3, 1H, S₂C₃H₆-H³), 2.69 (dq, *J* = 13, 3, 1H, S₂C₃H₆-H^{5/6}), 2.62 (dq, *J* = 13, 3., 1H, S₂C₃H₆-H^{5/6}), 2.53 (tq, *J* = 13, 3, 1H, S₂C₃H₆-H¹), 2.46 (d, 3H, *J* = 1.4, SCH₃), 1.58 (d, 9H, *J* = 10.2, Fe(CO)₃(PMe₃)), 1.58 (m, 1H, S₂C₃H₆-H⁴), (d, 9H, *J* = 10.8, Fe(SMe)(CO)₂(PMe₃)). ¹³C NMR (CD₂Cl₂): δ 220.4 (dd, *J*_{C-P} = 28.2, 5.7, μ-CO), 208.22 (dd, *J*_{C-P} = 17.2, 2.5, CO_{ap}), 204.54 (d, *J*_{C-P} = 11.9, CO_{ba}), 203.74 (d, *J*_{C-P} = 16.8, CO_{ba}), 161.72 (q, *J*_{C-B} = 49.7, BAr^F₄⁻), 134.7 (s, BAr^F₄⁻-ortho), 128.69 (q, *J* = 31.1, BAr^F₄⁻-meta), 124.5 (q, *J*_{C-F} = 272.64, BAr^F₄⁻), 117.5 (s, BAr^F₄⁻-para), 34.34 (s), 21.63 (dd, *J* = 5.3, 1.2), 18.8 (d, *J* = 4.6), 17.33 (s), 15.72 (d, *J*_{C-P} = 32.9, PMe₃), 15.03 (d, *J*_{C-P} = 36.4). Anal. Calcd for C₄₆H₃₉BF₂₄Fe₂O₄P₂S₃ (found): C, 39.68 (39.53); H, 2.46 (2.67); N, 0.0 (0.0).

Justification of ¹H NMR assignments for propanedithiolato protons: Integration indicated that only five protons were present in the typical propanedithiolate range (~4-2.5 ppm); six inequivalent protons are expected. The TOCSY experiment was performed in order to locate the sixth proton, which apparently overlaps with resonances of the PMe₃ ligands. A ¹H-¹³C HSQC experiment was used to determine which pairs of protons corresponded to a single methylene. The ³¹P-decoupled ¹H NMR spectrum was then used to identify the central methylene ligand, which is expected to not couple either phosphine; only one resonance (at 2.74 ppm) is unaffected when the the ³¹P decoupler is turned on, and we assume the other that is decoupled is buried under the PMe₃

resonances (1.58 ppm). In tandem, these experiments confirm that the dramatically upfielded shifted resonance (1.58 ppm) corresponds to the central methylene resonance, and we propose that this is due to an interaction with the apical carbonyl ligand. The NOESY experiment indicated that no through-space interaction is observed between the central methylene and the terminal methyl thiolate. Such an interaction is only expected if the central methylene is oriented towards the $\text{Fe}(t\text{-SMe})(\text{CO})_2(\text{PMe}_3)$ center rather than the $\text{Fe}(\text{CO})_3(\text{PMe}_3)$ center. Thus we propose that rapid chair flipping of the propanedithiolate ligand is not occurring at the temperature of this experiment (-20 °C). A through-space interaction was instead observed between the methyl thiolate and a single SCH_2 group, indicating which methylene is in proximity to the methyl thiolate and distinguishing between the axial and equatorial positions. However, we were unable to differentiate between the axial and equatorial protons on the remaining SCH_2 protons (facing away from the *t*-SMe).



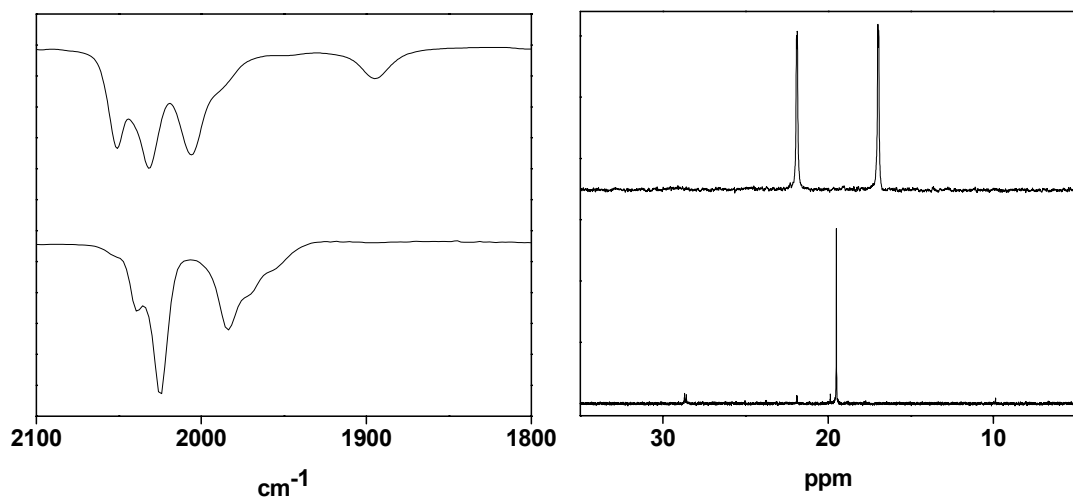


Figure SI-A2. Left: IR spectra (CH_2Cl_2) and of $[\mathbf{1}(t\text{-SMe})]^+$ (top) and $[\mathbf{1}(\mu\text{-SMe})]^+$ (bottom). Right: $^{31}\text{P}\{\text{H}\}$ spectra (CD_2Cl_2) of $[\mathbf{1}(t\text{-SMe})]^+$ (top) and $[\mathbf{1}(\mu\text{-SMe})]^+$ (bottom).

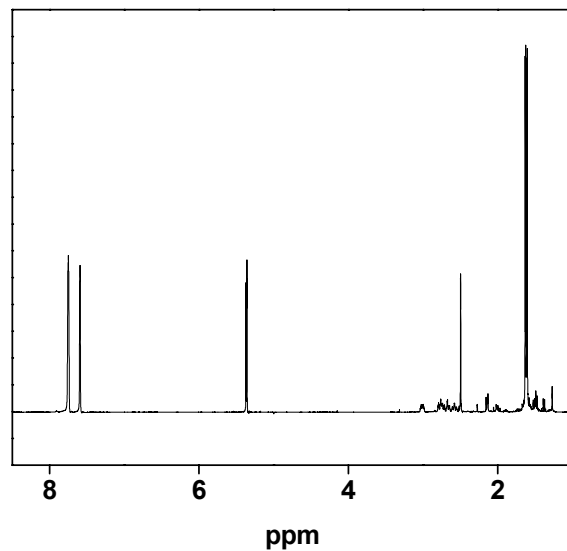


Figure SI-A3. 500 MHz ^1H NMR spectrum (CD_2Cl_2 , -15 °C) of $[\mathbf{1}(t\text{-SMe})]\text{BAr}_4^F$.

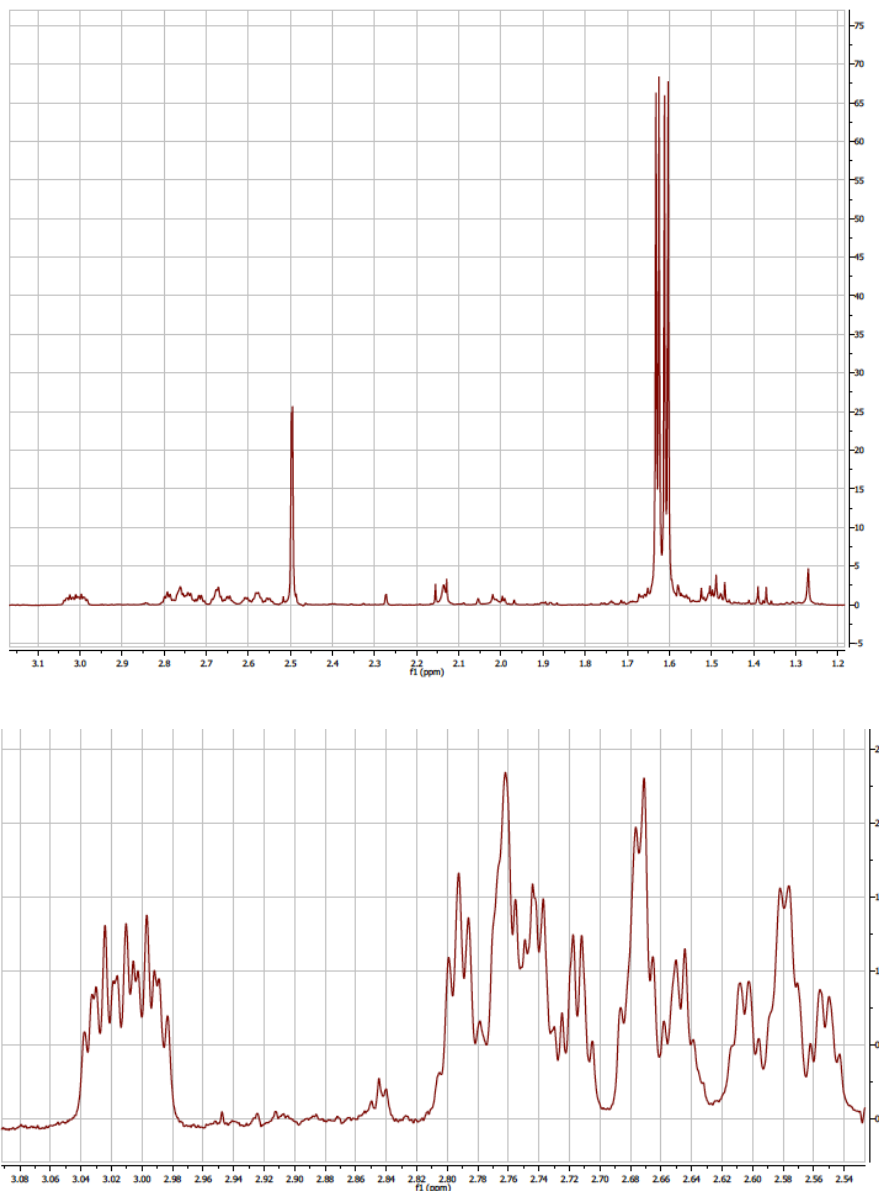


Figure SI-A4. 500 MHz ^1H NMR spectrum (CD_2Cl_2 , -15°C) of $[\mathbf{1}(t\text{-SMe})]\text{BAr}^{\text{F}}_4$ in the region δ 3.0 to 1.2. Signals assigned the methylene groups are depicted in the expanded spectrum at the bottom.

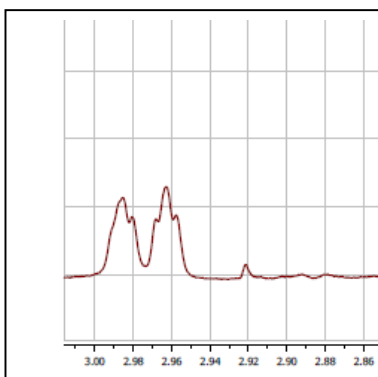


Figure SI-A5. 600 MHz $^1\text{H}\{^{31}\text{P}\}$ NMR spectrum of $[\mathbf{1}(t\text{-SMe})]\text{BAr}^{\text{F}}_4$ (CD_2Cl_2 , -20°C). ^{31}P decoupling is observed at all resonances shown except for the one at 2.74 ppm. Apparently, ^{31}P coupling to both PMe_3 ligands is observed on many protons of the propanedithiolato

ligand. This pattern is consistent with this resonance corresponding to the central methylene.

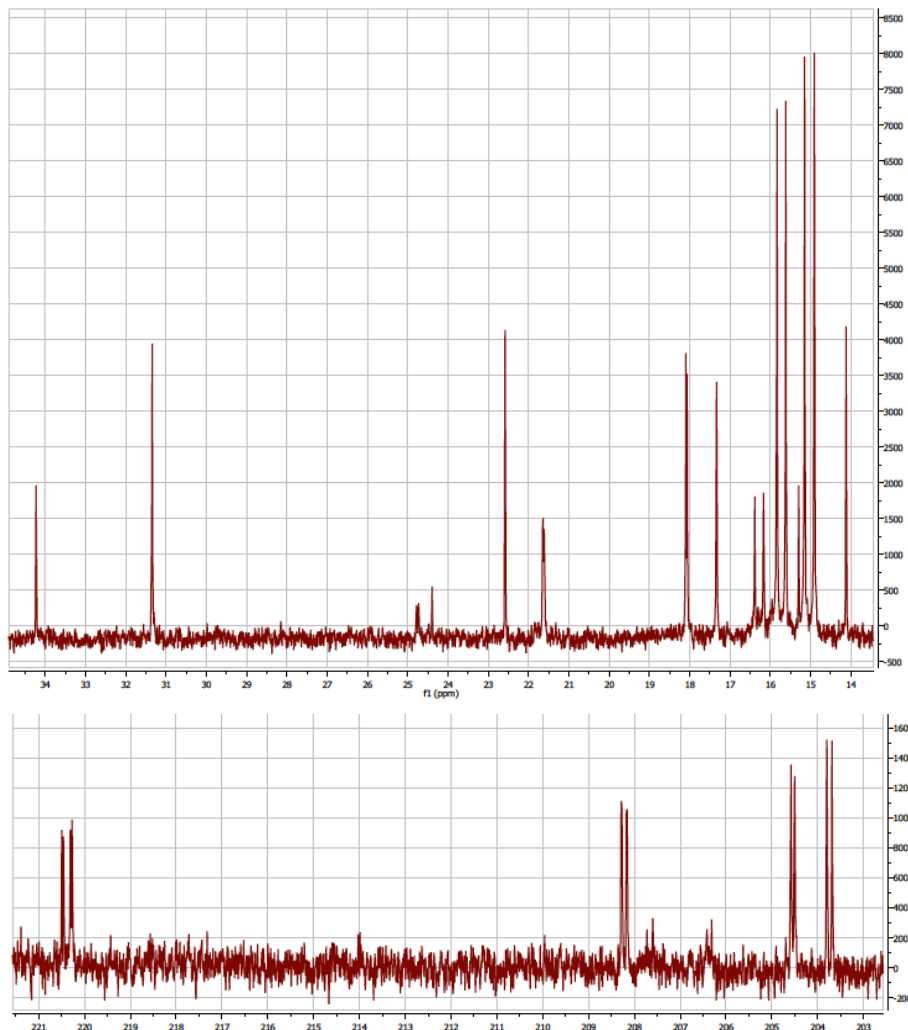


Figure SI-A6. 150.8 MHz $^{13}\text{C}\{\text{H}\}$ NMR spectrum of $[\mathbf{1}(t\text{-SMe})]\text{BAr}^{\text{F}_4}$ (CD_2Cl_2 , -30 °C) in the high field (top) and FeCO regions. In the full spectrum, signals at δ 32, ~21.5, and 14 arise from pentane, the signal at δ ~15.25 is Et_2O , the doublet at δ ~16.25 and singlets at ~24.5 are from a small amount of $[\mathbf{1}(\mu\text{-SMe})]\text{BAr}^{\text{F}_4}$. In the low-field spectrum notice four diastereotopic CO ligands, each coupled to ^{31}P . The low field signal is assigned to $\mu\text{-CO}$. This signal displays two resolvable couplings to ^{31}P .

[Fe₂(pdt)(μ-SMe)(CO)₄(PMe₃)₂]BAr^F₄. The bridging sulfide complex (the BF₄⁻ salt has been described: I. P. Georgakaki, M. L. Miller and M. Y. Darenbourg, *Inorg. Chem.*, 2003, **42**, 2489) was generated by simply warming solutions of the terminal thiolate to room temperature. ^1H NMR characterization was not previously reported. ^1H NMR (CD_2Cl_2): δ 7.72 (m, 8H, BAr^F₄⁻), 7.62 (bs, 4H, BAr^F₄⁻), 2.84 (tt, 2H, J = 6.8, 1.3,

($\text{SCH}_2)_2\text{CH}_2$), 2.78 (m, 2H, ($\text{SCH}_2)_2\text{CH}_2$), 2.41 (p, $J_{\text{H-H}} = 6.8$, ($\text{SCH}_2)_2\text{CH}_2$), 2.27 (t, $J_{\text{H-P}} = 0.8$, SCH_3), 1.51 (d, 18H, $J_{\text{H-P}} = 10.2$, PMe_3). ^{13}C NMR (CD_2Cl_2 , -30 °C): δ 207.59 (dd, $J_{\text{C-P}} = 22.9$, 3.7, FeCO), 206.14 (dd, $J_{\text{C-P}} = 18.5$, 3.9), 161.66 (q, $J_{\text{C-B}} = 49.7$, $\text{BAr}^{\text{F}}_4^-$), 134.66 (s, $\text{BAr}^{\text{F}}_4^-$ -ortho), 128.65 (q, $J = 31.1$, $\text{BAr}^{\text{F}}_4^-$ -meta), 124.46 (q, $J_{\text{C-F}} = 272.64$, $\text{BAr}^{\text{F}}_4^-$), 117.53 (s, $\text{BAr}^{\text{F}}_4^-$ -para), 24.72 (d, $J_{\text{C-P}} = 8.6$, SCH_3), 24.37 (s, ($\text{SCH}_2)_2\text{CH}_2$), 16.22 (d, $J_{\text{C-P}} = 32.9$, PMe_3), 15.91 (s, ($\text{SCH}_2)_2\text{CH}_2$).

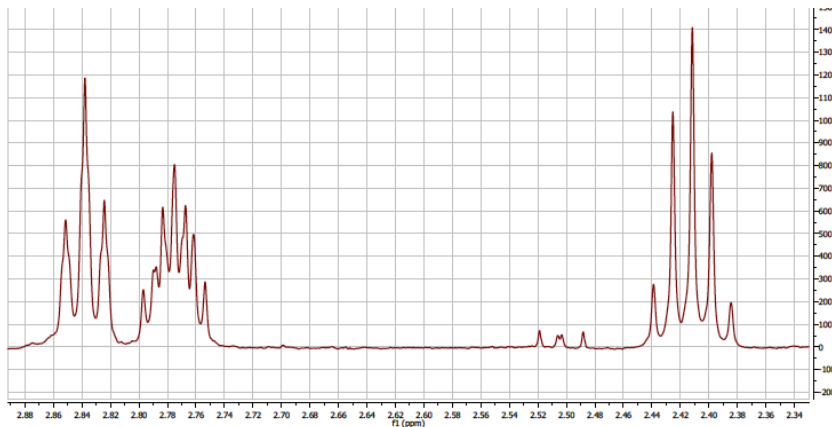
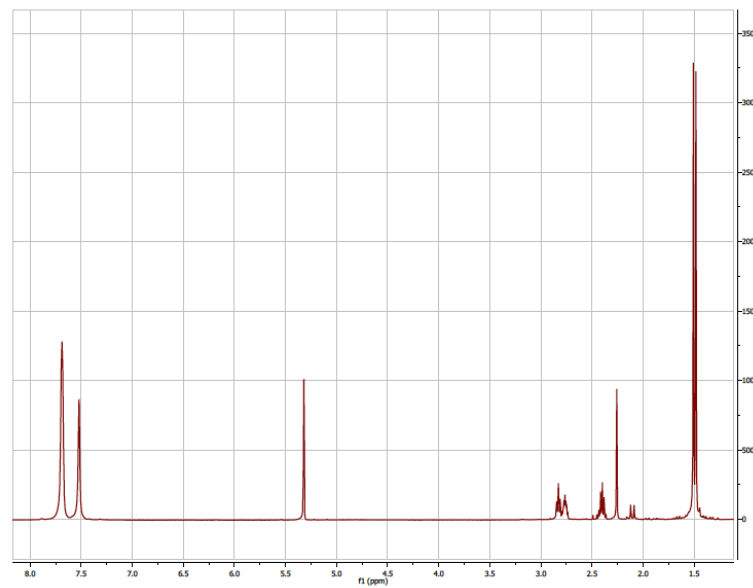


Figure SI-A7. 500 MHz ^1H NMR spectrum (CD_2Cl_2 , 20 °C) of $[1(\mu\text{-SMe})]\text{BAr}^{\text{F}}_4$, full scale (top) and expansion of the methylene region (bottom).

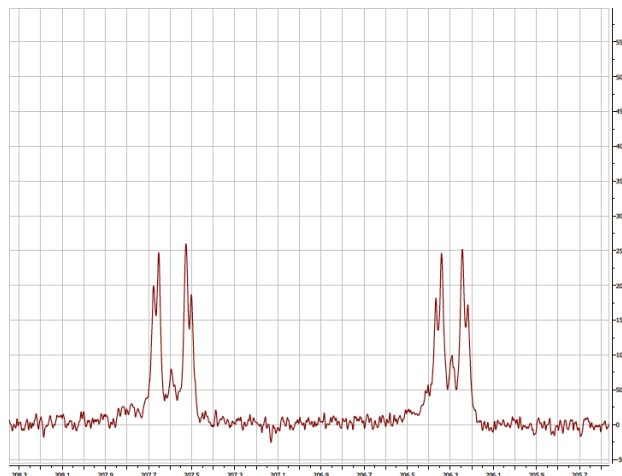


Figure SI-A8. 150.8 MHz $^{13}\text{C}\{\text{H}\}$ NMR spectrum of $[\mathbf{1}(\mu\text{-SMe})]\text{BAr}^{\text{F}}_4$ (CD_2Cl_2) in the FeCO region.

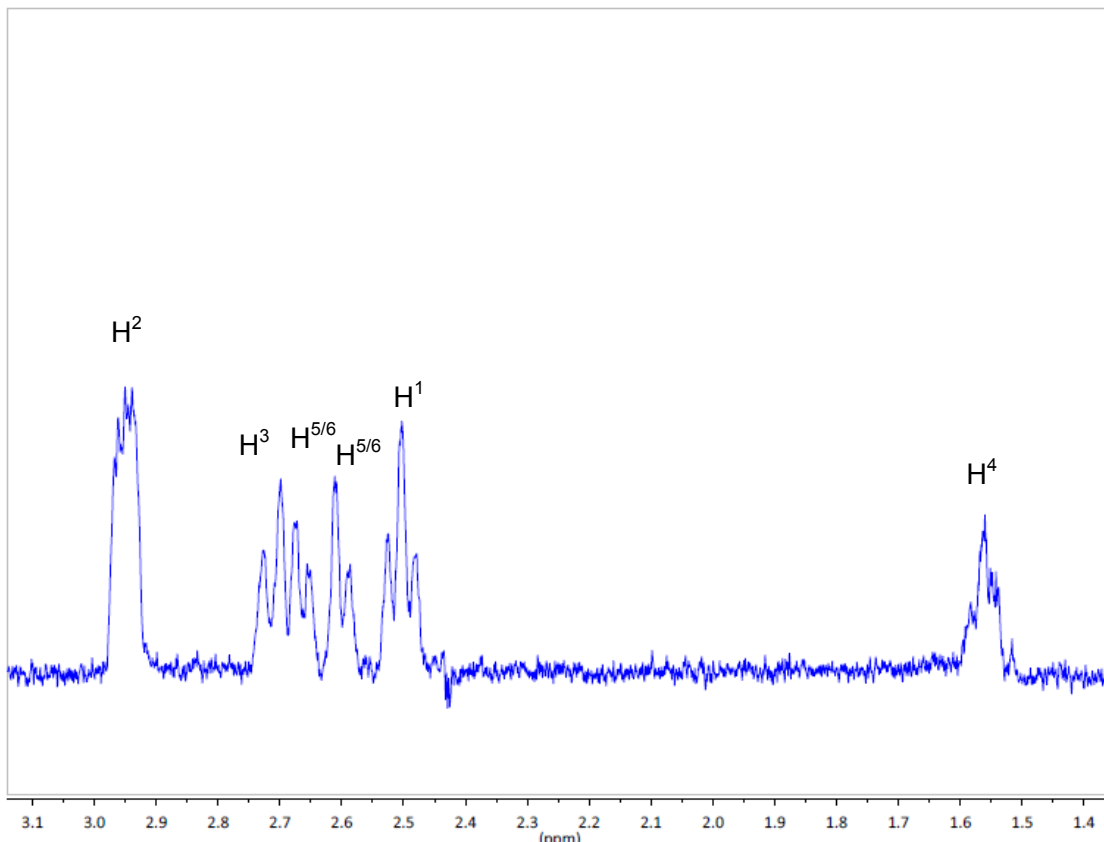


Figure SI-A9. 600 MHz ^1H NMR TOCSY spectrum (CD_2Cl_2 , -20 °C) of $[\mathbf{1}(t\text{-SMe})]\text{BAr}^{\text{F}}_4$. Irradiation was centered at 2.5 ppm with 0.4 s of mixing time. This experiment is consistent with a ^1H resonance from the propanedithiolato ligand being buried underneath the Fe- PMe_3 resonances.

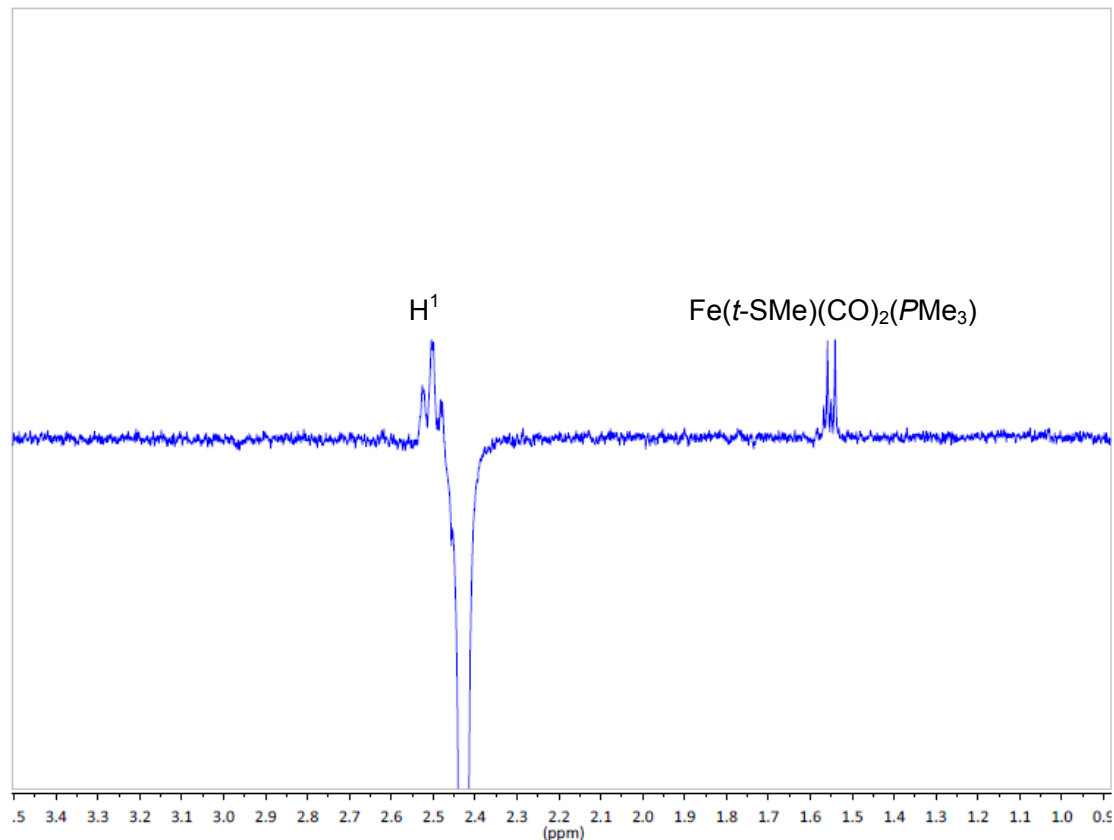


Figure SI-A10. 600 MHz 1D NOESY spectrum of $[1(t\text{-SMe})]\text{BAr}^{\text{F}_4}$. Irradiation was centered at 2.43 ppm, which corresponds to the resonance of the terminal methyl thiolato ligand.

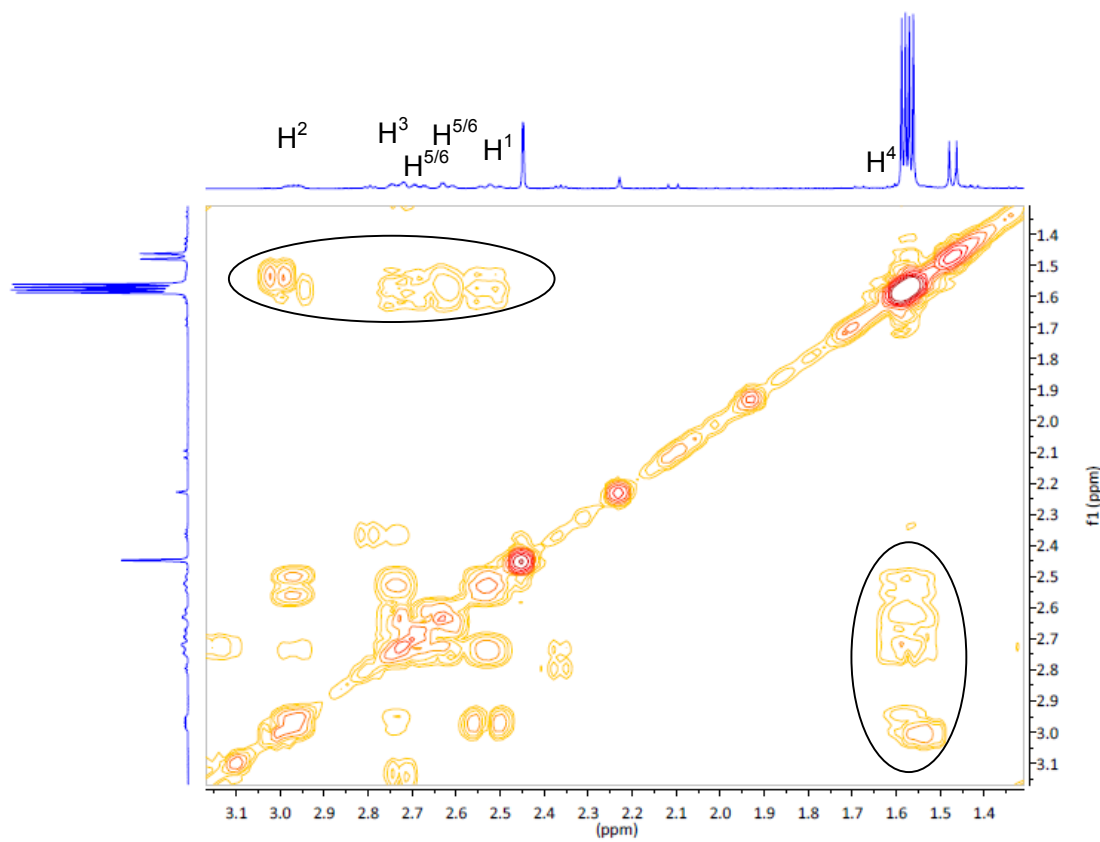


Figure SI-A11. ^1H – ^1H COSY spectrum (CD_2Cl_2 , -20°C) of $[\mathbf{1}(t\text{-SMe})]\text{BAr}_4^{\text{F}}$.

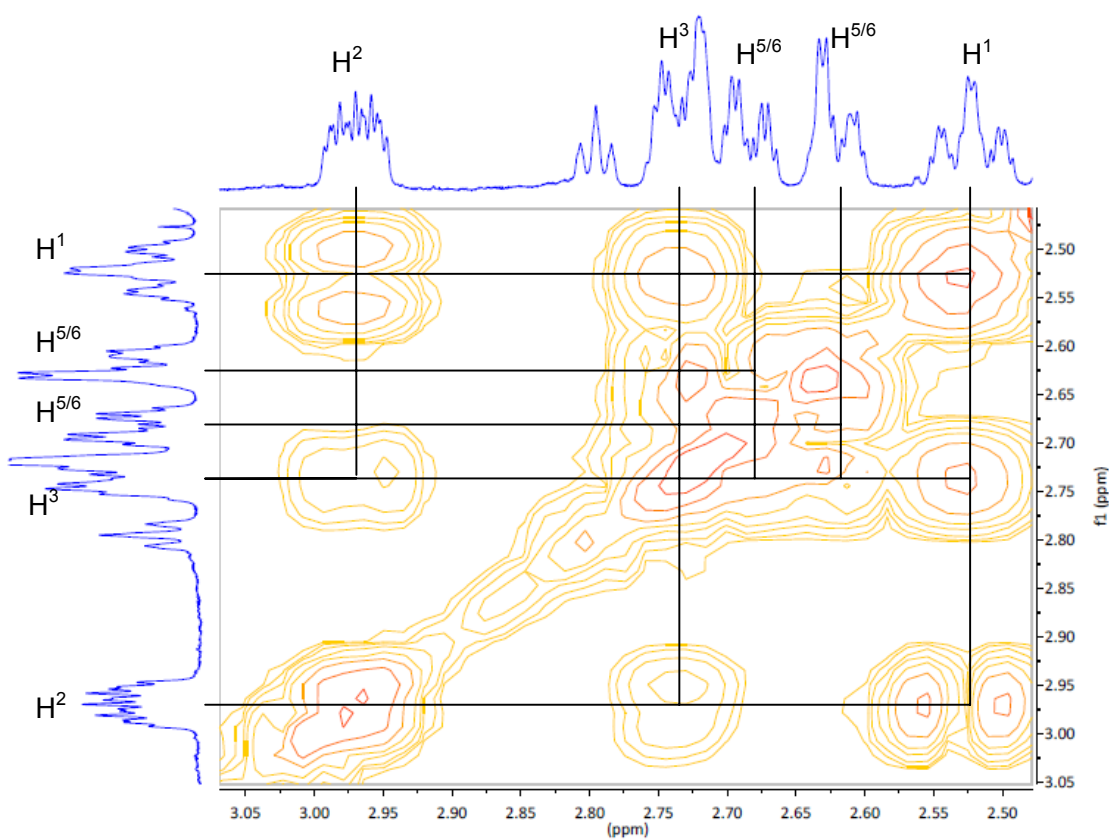


Figure SI-A12. ^1H - ^1H COSY spectrum (CD_2Cl_2 , -20°C) of $[1(t\text{-SMe})]\text{BAr}^{\text{F}}_4$, zoomed in view.

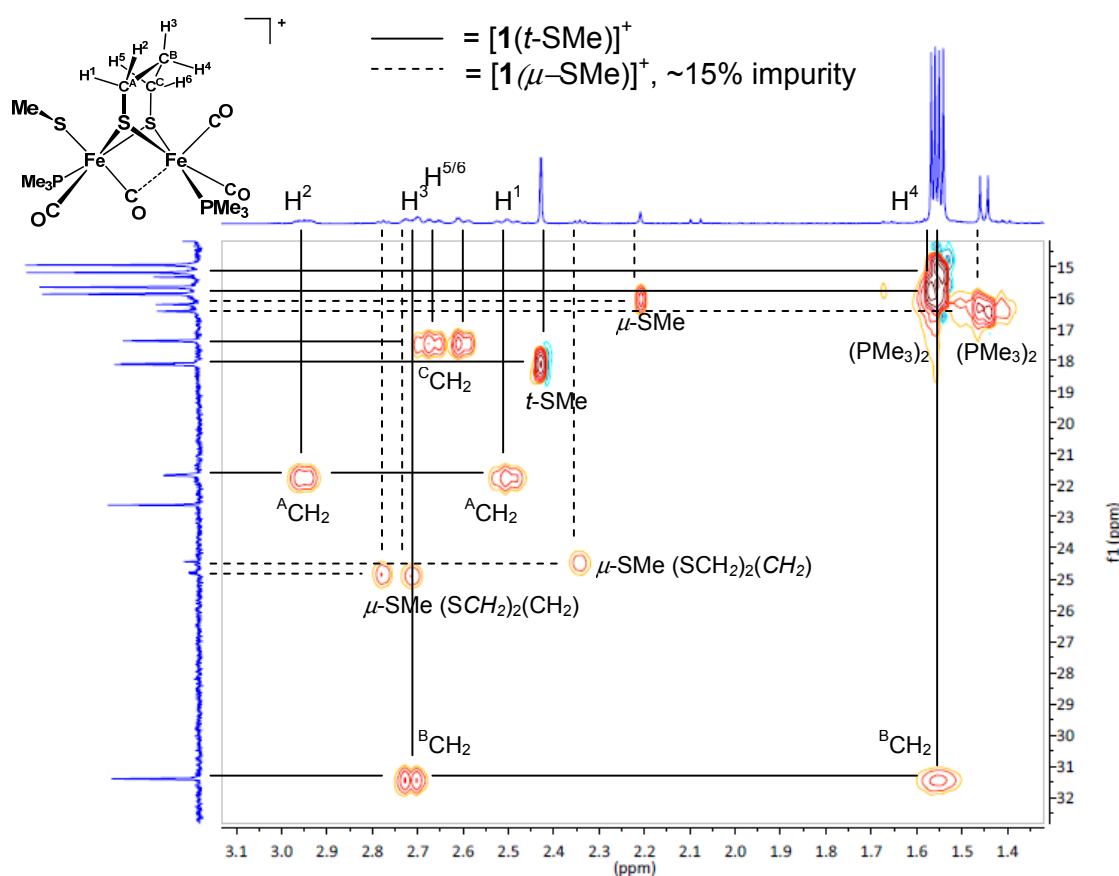


Figure SI-A13. ^1H - ^{13}C HSQC spectrum of $[1(t\text{-SMe})]\text{BArF}_4$ with assignments.

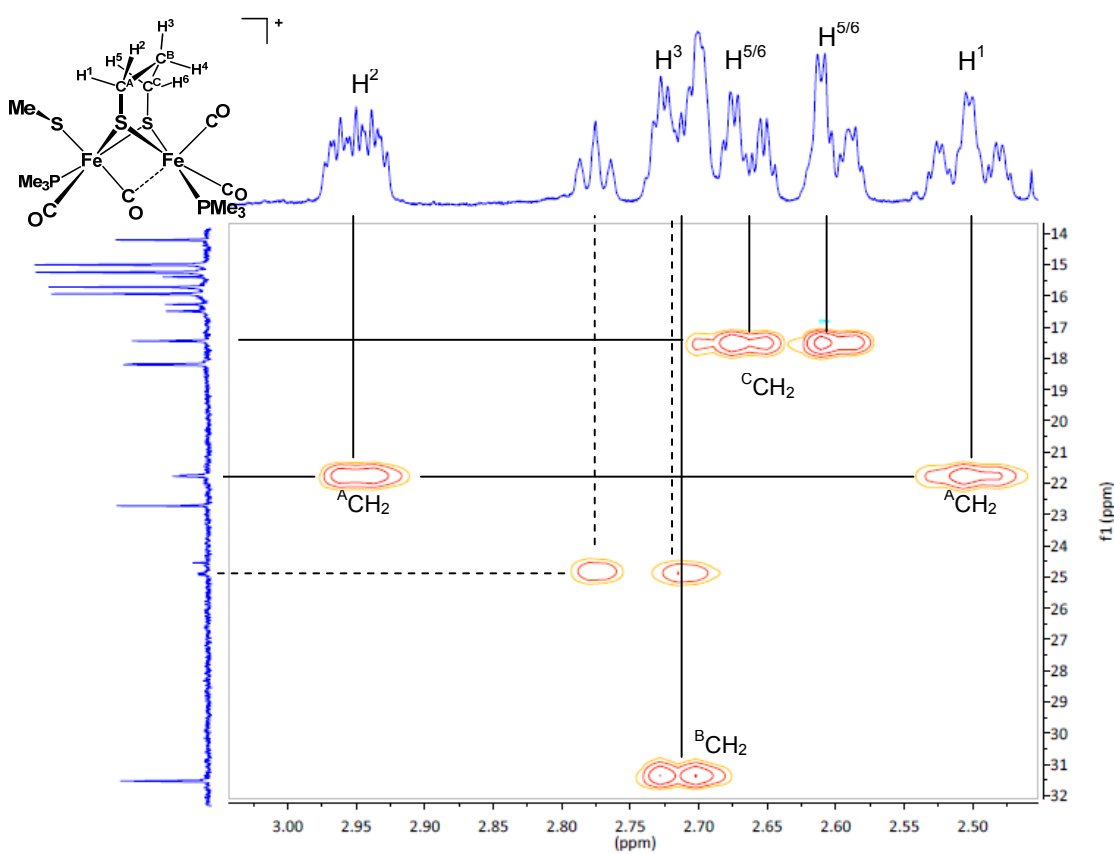


Figure SI-A14. ^1H – ^{13}C HSQC spectrum of $[\mathbf{1}(t\text{-SMe})]\text{BAr}^{\text{F}}_4$, expanded view.

I.B. Kinetic Measurements

In a typical experiment, 0.006 g of $[\text{Fe}_2(\text{pdt})(t\text{-SMe})(\text{CO})_4(\text{PMe}_3)_2]\text{BAr}^{\text{F}}_4$ and 0.0005 g of trimethoxybenzene (internal standard) were added to a J. Young valve NMR tube, dissolved in 0.75 mL of CD_2Cl_2 . The solution was immediately cooled to -78°C . The tube was then inserted into a spectrometer, the probe of which was set at the appropriate temperature. After ~ 5 min of equilibration, data acquisition was initiated. Arrays of ^1H NMR were collected for 2-4 h. Post-experiment, the Fe-SMe resonances for the reactant and product were integrated versus the internal standard and plotted vs time. Calibration of the temperature inside the spectrometer was performed with a standard of pure MeOH post-reaction.

Conditions:

Sweep width: 10 – 0 ppm

Number of transients: 10

Delay between scans: 1s

Total acquisition time per transient: 4.0816 s

Table SI-B1. Rate constants from fitted plots of concentration vs time for the isomerization of $[1(t\text{-SMe})]^+$ to $[2(\mu\text{-SMe})]^+$. Temperatures of the NMR probe were calibrated with methanol.

k (s⁻¹)	T (K)	graphic
1.76E-04	292.45	Figure SI-B2
2.54E-04	294.25	Figure SI-B3
4.30E-04	298.45	Figure SI-B4
9.96E-04	302.95	Figure SI-B5
1.53E-03	307.55	Figure SI-B6

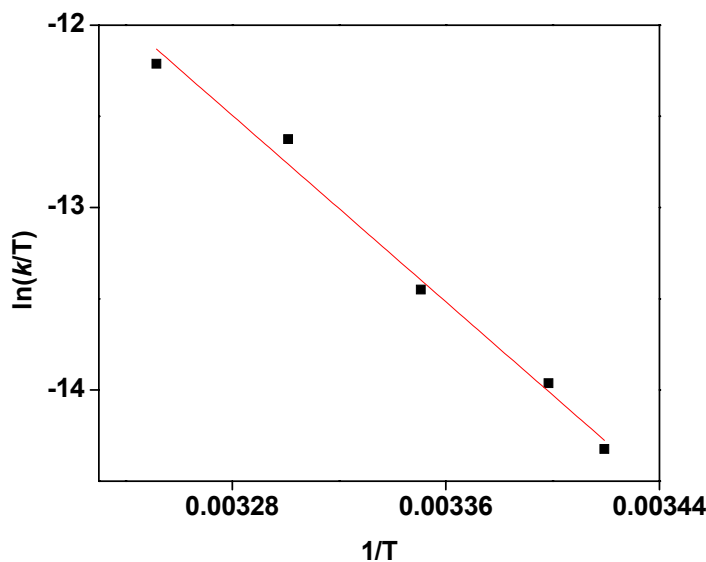


Figure SI-B1. Eyring-Polanyi plot for the isomerization of $[1(t\text{-SMe})]\text{BAr}_4^{\text{F}}$ to $[1(\mu\text{-SMe})]\text{BAr}_4^{\text{F}}$. The equation linear fit of the data (red line) is $y = -12776x + 29.412$ with $R^2 = 0.9898$.

Calculation of ΔH^\ddagger :

$$\text{slope} = -12776 = \Delta H^\ddagger/R = \Delta H^\ddagger/8.314$$

On the basis of 5 data points, the OriginLab graphing program calculates error of 6% in the slope.

$$\Delta H^\ddagger = 106225.7 \text{ J/mol K} = 25.4 \text{ kcal/mol K}$$

Calculation of ΔS^\ddagger :

$$\text{y-intercept} = 29.412 = \ln(k_B/h) + (\Delta S^\ddagger/R) = \ln(1.38 \times 10^{-23}/6.63 \times 10^{-34}) + (\Delta S^\ddagger/8.314)$$

On the basis of 5 data points, the OriginLab graphing program calculates error of 10% in the intercept.

$$\Delta S^\ddagger = 47.0 \text{ J/K} = 1.12 \text{ kcal/K.}$$

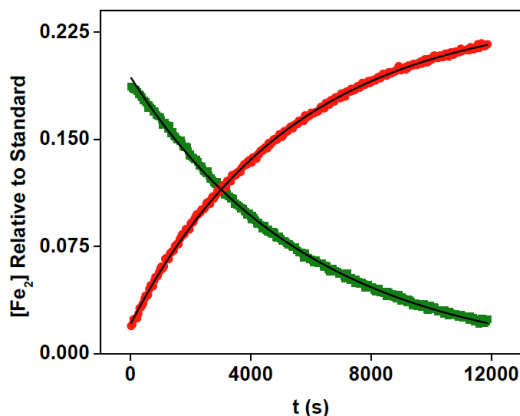


Figure SI-B2. Plot of concentration vs time for the isomerization of $[1(t\text{-SMe})]^+$ to $[2(\mu\text{-SMe})]^+$ (CD_2Cl_2 , 292 K). The fits are shown in black.

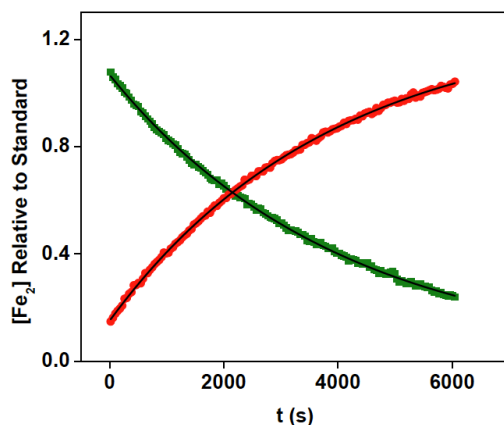


Figure SI-B3. Plot of concentration vs time for the isomerization of $[1(t\text{-SMe})]^+$ to $[2(\mu\text{-SMe})]^+$ (CD_2Cl_2 , 294 K). The fits are shown in black.

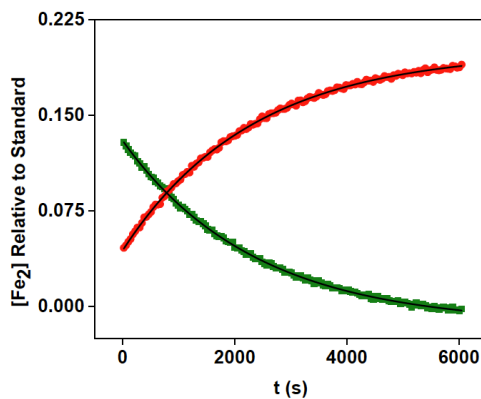


Figure SI-B4. Plot of concentration vs time for the isomerization of $[1(t\text{-SMe})]^+$ to $[2(\mu\text{-SMe})]^+$ (CD_2Cl_2 , 298 K). The fits are shown in black.

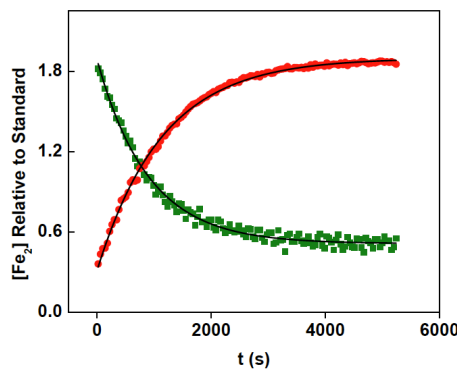


Figure SI-B5. Plot of concentration vs time for the isomerization of $[1(t\text{-SMe})]^+$ to $[2(\mu\text{-SMe})]^+$ (CD_2Cl_2 , 303 K). The fits are shown in black.

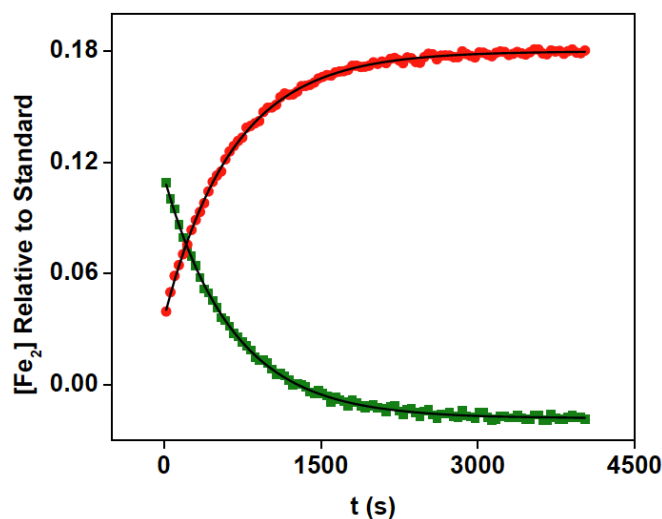


Figure SI-B6. Plot of concentration vs time for the isomerization of $[1(t\text{-SMe})]^+$ to $[2(\mu\text{-SMe})]^+$ (CD_2Cl_2 , 308 K). The fits are shown in black.

Part II. Computational Results

II.A. Methods

Density functional theory (DFT) calculations have been performed by using the TURBOMOLE suite of programs¹. Minimum energy points and transition states have been located on the Potential Energy Surface of the B-P86/TZVP^{2,3} level of functional/basis set protocol. This level of theory has been shown to be suited to reliably investigate [FeFe] hydrogenase models.⁴⁻⁶

Saddle and minimum points on the PES have been determined by means of energy gradient techniques and a full vibrational analysis has been carried out to further characterize each stationary point. The optimization of transition state structures has been carried out according to a procedure based on a pseudo-Newton-Raphson method. First, geometry optimization of a guess transition state structure is carried out by constraining the distance corresponding to the reaction coordinate (RC).

After performing the vibrational analysis at BP86/TZVP level of the constrained minimum energy structures, the negative eigenmode associated to the RC is then followed to locate the true transition state structure, i.e. the maximum energy point along the trajectory, which joins two adjacent minima.

Gibbs free energy (G) values have been obtained from the electronic SCF energy considering three contributions to the total partition function (Q), namely $q_{\text{translational}}$, $q_{\text{rotational}}$, $q_{\text{vibrational}}$, under the assumption that Q may be written as the product of such terms. In order to evaluate enthalpy and entropy contributions, the values of temperature and pressure have been set to 23 °C and 1 bar, respectively, to reproduce as closely as possible experimental conditions. Rotations have been treated classically and vibrational modes described according to the harmonic oscillator approximation.

An implicit treatment of solvent effect (COSMO,⁷ $\sigma = 9.1$, dichloromethane) has been used to correct gas phase energy values in order to check substantial differences possibly existing between energy values computed in gas phase/solvent conditions. Determined correction values are, however, lower than precision limit of the computational method.

In light of available experimental data and considering the chemical nature of the ligands, only low-spin species have been investigated.

1. Ahlrichs, R.; Bar, M.; Haser, M.; Horn, H.; Kolmel, C., *Chem. Phys. Lett.* **1989**, *162*, 165-169.
2. Becke, A. D., *Phys. Rev A* **1988**, *38*, 3098-3100.
3. Perdew, J. P., *Phys Rev B Condens. Matter* **1986**, *33*, 8822-8824.
4. Bertini, L.; Bruschi, M.; de Gioia, L.; Fantucci, P.; Greco, C.; Zampella, G., *Atomistic Approaches in Modern Biology: From Quantum Chemistry to Molecular Simulations* **2007**, *268*, 1-46.
5. Bruschi, M.; Zampella, G.; Fantucci, P.; De Gioia, L., *Coord. Chem. Rev.* **2005**, *249*, 1620-1640.
6. Zampella G., Greco C.; Fantucci P., De Gioia, L. *Inorg. Chem.* **2006**, *45*, 4109-4118.
7. Schafer, A.; Klamt, A.; Sattel, D.; Lohrenz, J. C. W.; Eckert, F., *Phys. Chem. Chem. Phys.* **2000**, *2*, 2187-2193.

II.B. Ground state structures and HOMOs.

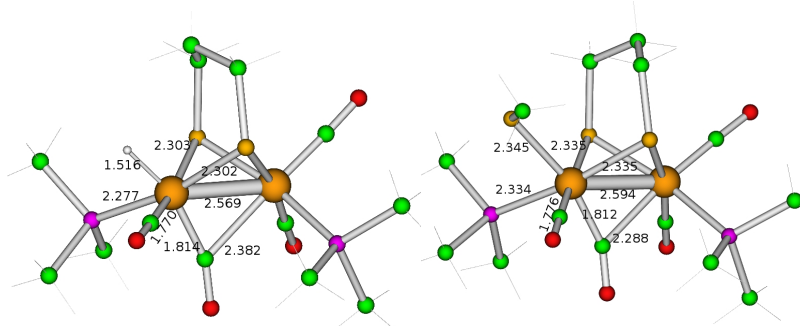


Figure SII-B1. DFT optimized structures of terminal hydride ($[1(t\text{-H})]^+$, left) and terminal SMe derivative ($[1(t\text{-SMe})]^+$, right). Distances are in Å.

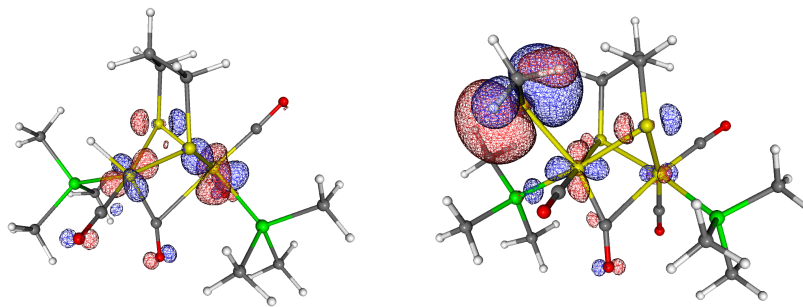
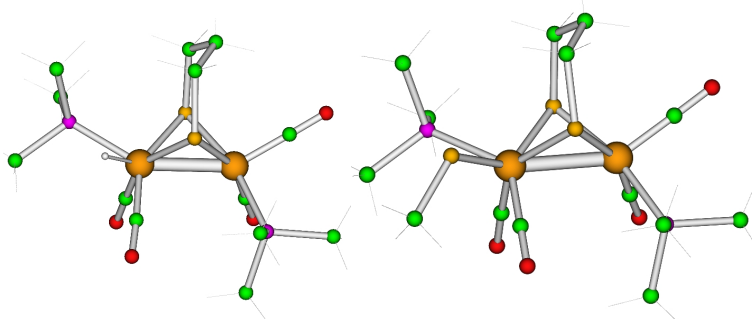


Figure SII-B2. HOMO for terminal hydride ($[1(t\text{-SMe})]^+$, left) and terminal SMe derivative ($[1(t\text{-SMe})]^+$, right).

II.C. First transition state structures and HOMOs.



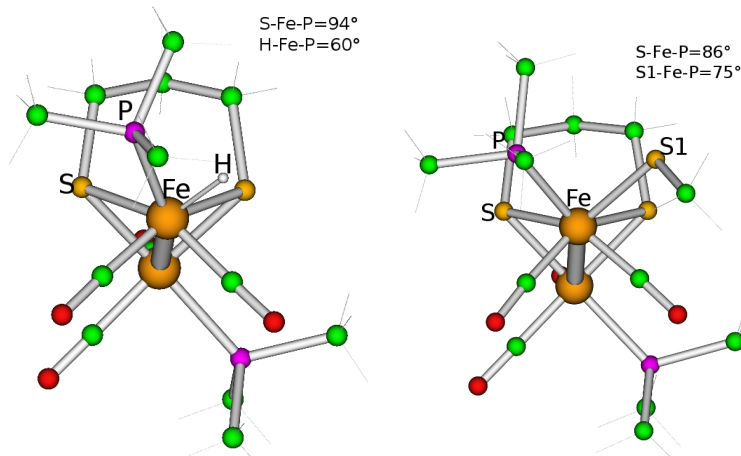


Figure SII-C1. DFT optimized structures (rhombic or trigonal prisms) of Ray-Dutt transition states that are associated to the first step (rate determining) of nondissociative rearrangement leading from terminal axial coordinated isomers to bridging ones (via the terminal basal isomers). On the left a double view has been shown of the TS associated with the SMe derivative whereas on the right the same holds true for the hydride. Bottom: a perspective along-Fe-Fe-bond that highlights angular differences that reflect the differing sizes of H vs SMe.

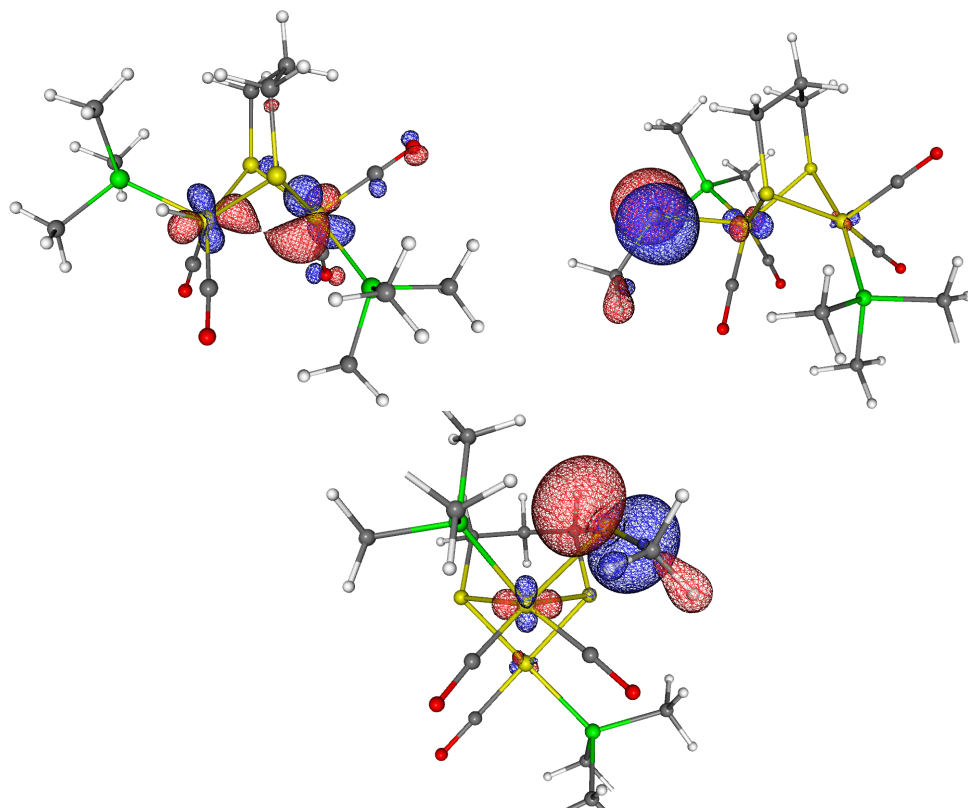


Figure SII-C2. HOMO for transition state for ($[1(t\text{-H})]^+$, top left) and terminal SMe derivative ($[1(t\text{-SMe})]^+$, top right and bottom right, two view points presented).

II.D. Transition states for isomerization after formation of μ -SMe and μ -H.

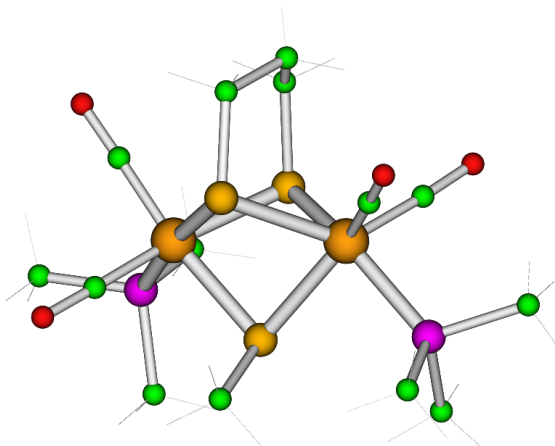


Figure SII-D1. Calculated Bailar twist transition state for the isomerization of $[1(\mu\text{-SMe})]^+$ from the isomer in which the PMe₃ ligands are cisoid dibasal (observed final product) to an isomer in which the PMe₃ ligands are transoid dibasal. Steric clashing between the μ -SMe ligand and PMe₃ ligand of the rotating Fe(CO)₂(PMe₃) center is proposed to account for the high barrier towards this isomerization, as well as the energetically uphill location of the product. Note that in the case of the hydride, the cisoid dibasal PMe₃ isomer is the final observed product.

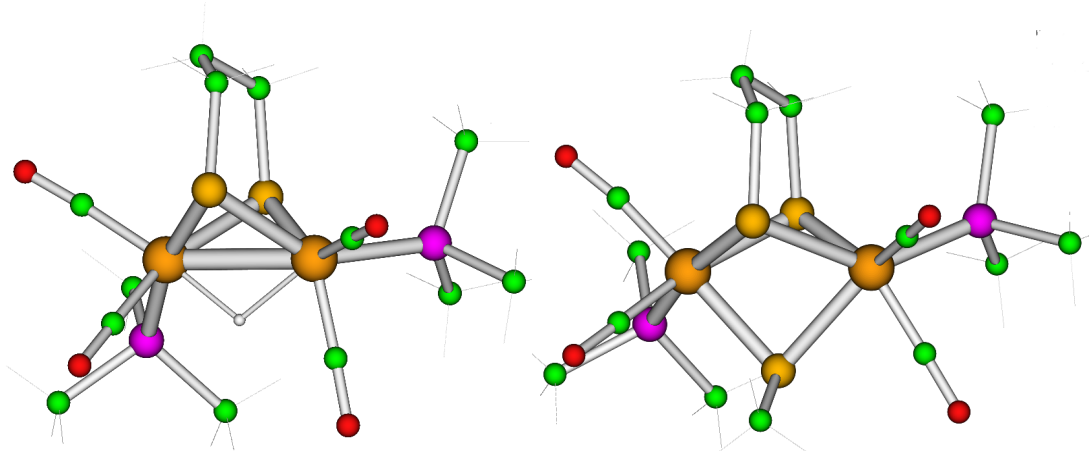


Figure SII-D2. Calculated Bailar twist transition state for the isomerization of $[1(\mu\text{-H})]^+$ (left) and $[1(\mu\text{-SMe})]^+$ (right) from a structure where the PMe₃ ligands are cisoid-dibasal to apical-basal. In the case of $[1(\mu\text{-SMe})]^+$, this process is uphill and thus not observed. In the case of the $[1(\mu\text{-H})]^+$, the *initially observed* product of protonation (of **1**) contains apical-basal PMe₃ ligands, which convert to the transoid dibasal PMe₃ isomer upon warming; unlike the methylsulfide complex, a cisoid dibasal PMe₃ ligand is not observed. The above transition state may account for an alternative isomerization mechanism in

which the cisoid dibasal PMe₃ isomer is first formed and then rapidly isomerizes to the apical-basal PMe₃ isomer.